Artificial Intelligence Based Hyper-parameter Adjustment on Deep Neural Networks: An Application of Detection and Classification of COVID-19 Diseases

Suresh Srirangam
Email: shamprasads@gmail.com

_____

Abstract: Earlier diagnosis of COVID-19 using radiological images become a challenging task in the healthcare sector. The recent development of artificial intelligence (AI) methods find useful for the investigation of radiological images to accomplish accurate COVID-19 diagnosis in an automated way. With this motivation, this paper presents an AI based hyper-parameter adjustment on deep neural networks (AIHA-DNN) technique for COVID-19 diagnosis and classification. The AIHA-DNN technique focuses on detecting the existence of COVID-19 utilizing CXR (CXR) images. The AIHA-DNN technique involves the Weiner filtering (WF) based pre-processing technique to get rid of the noise that exists in the Chest X-ray (CXR) image. Then, the Squeeze Net based feature extractor is utilized to derive a useful set of feature vectors. Moreover, improved grey wolf optimization based deep neural network (IGWO-DNN) technique is used for the classification of CXR images into proper class labels. The IGWO algorithm is utilized for the hyper-parameter adjustment of the DNN model to accomplish maximum detection rate. The performance validation of the AIHA-DNN technique takes place on benchmark CXR datasets and the experimental values are examined with respect to different measures. The simulation outcomes reported the supremacy of the AIHA-DNN technique over the recent methods with the maximum sensitivity, specificity, and accuracy of 97.69%, 96.65%, and 97.61% respectively.

Keywords: Artificial intelligence, Radiologists, Chest X-ray, Deep learning, Hyperparameter tuning.
_____

1. Introduction

The presentation of COVID-19 is started by reporting of unidentified cause of pneumonia in Wuhan, Hubei region of China on December 31, 2019, has rapidly turn into an epidemic [1, 2]. The disease is called COVID-19 and the virus is named SARS-CoV-2. The usual medical signs of COVID-19 include cough, fever, headache, sore throat, muscle pain, shortness of breath, and fatigue [3]. Currently, the most popular test method utilized for diagnosing COVID-19 is a RT-PCR test. Chest radiological imaging plays a major part in earlier diagnoses and treatment of this disease [4, 5]. At an early stage of pandemic, Chinese medical centres had inadequate test kits that are also generating a higher rate of false negative outcomes, hence physicians are stimulated for making diagnoses on the basis of chest CT and medical outcomes [6]. CT is broadly utilized for detecting COVID-19 in which a lower amount of test kits at the beginning of epidemic have been presented. Scientists state that integrating medical image features with lab results might assist in earlier detection of COVID-19. Radiologic images attained from COVID-19 patients have beneficial data for diagnosis. Few researchers have faced modifications in CT images and CXRs beforehand the start of COVID-19 indications. Applications of ML method for automated diagnoses in the field of medicine have become more popular by an adjunct tool for physicians. DL is a field of AI, allows making of dedicated modules for achieving significant results by the input data, without requiring manual feature extraction.

DL methods have been effectively employed in several challenges like skin cancer classification, arrhythmia detection, brain disease classification, lung segmentation, fundus image segmentation, pneumonia diagnosis from CXR images, etc. The COVID-19 pandemic rapidly increases the requirement for experts in this field. This has improved attention in emerging the automatic detection system on the basis of AI methods. It is a difficult process for providing skilled physicians to all the hospitals because of the constrained amount of radiotherapists. Thus, fast, simple, and accurate AI approaches find helpful for overcoming these problems and offer timely maintenance for the patient. Though radiotherapists perform a major part because of their considerable expertise in this domain, the AI techniques in radiology could be supportive for obtaining precise diagnoses. In addition, AI methods could be beneficial in removing drawbacks like inadequate amount of available waiting time, rapid testing kit, expenses, etc.

This paper presents an AI based hyper parameter adjustment on deep neural networks (AIHA-DNN) technique for COVID-19 diagnosis. The AIHA-DNN technique involves the Weiner filtering (WF) based pre-

processing technique for the noise removal process. Besides, the Squeeze Net based feature extractor is used for the extraction of feature vectors. Furthermore, improved grey wolf optimization based deep neural network (IGWO-DNN) technique is employed to classify the CXR images into proper class labels. The IGWO algorithm is utilized for the hyper parameter adjustment of the DNN model to accomplish maximum detection rate. To investigate the classification efficacy of the AIHA-DNN technique, a series of simulations take place on benchmark CXR dataset, and the experimental values are investigated in terms of different measures.

2. Literature Review

Shah et al. [7] emphases on the classificaiton of COVID-19 using distinct DL models on CT images. A new CTnet-10 is created for diagnosing COVID-19. Loey et al. [8], presented a hybrid module utilize classical and deep ML method for detecting face mask. The projected method contains 2 modules. The initial module is created for extracting features with the help of Resnet50. Whereas the next module is created for processing classification of face masks with help of DT, SVM, and ensemble method. Jain et al. [9] captured the PA analysis of CXR scans for covid-19 infected and healthier persons. Afterward, clean up the images and apply data augmentation, they are utilized DL based CNN methods and related to efficiency. They have related ResNeXt, Inception V3, and Xception methods and studied their accuracy. In Ozturk et al. [10], a novel method for detecting automated COVID-19 onraw CXR image is introduced. Brunese et al. [11] proposed a method made up of 3 stages: the primary phase is for detecting CXR if it is existence of pneumonia. The next phase is for discerning among pneumonia and COVID-19. The final one is intended for localizing the area in the X ray symptomatic of COVID-19 existence.

In Pathak et al. [12], a deep TL method is utilized for classifying COVID-19 diseased persons. In addition, the top two smooth loss functions using cost sensitive attributes are also used for handling imbalanced and noisy COVID-19 dataset issues. Pustokhin et al. [13] presented a novel ResNet based Class Attention Layer using Bidirectional LSTM is named RCAL-BiLSTM for COVID-19 Diagnoses. The projected RCAL-BiLSTM method includes a sequence of methods like softmax (SM) based classification, RCAL-BiLSTM based feature extraction, and bilateral filtering (BF) based pre-processing. When the BF method generates the pre-processing image, RCBi-LSTM module, ResNet based feature extraction, and CAL are involved. Lastly, the SM layer is employed for categorizing the feature vector to respective feature map.

3. The AIHA-DNN Model

The AIHA-DNN model encompasses WF based preprocessing, SqueezeNet based feature extraction, DNN based classification, and IGWO based parameter adjustment. The detailed working of the AIHA-DNN model with its different subprocesses is elaborated in the succeeding sections.

3.1. Image Pre-processing

Noise removal in the image pre-processing function enhances the feature of an image, disturbed by noise. In detail, the adaptive filter was utilized that performs denoising process in the images. In Eq. (1), consider the image as $\hat{I}(x, y)$ but the noise difference of whole images are represented as σ_y^2. At this point, a local mean $\widehat{\mu_L}$ in the pixel window and local difference from window was signified as $\hat{\sigma}_y^2$. Then, the feasible method of image denoising is determined as follows:

$$\hat{\hat{I}} = \hat{I}(x, y) - \frac{\sigma_y^2}{\hat{\sigma}_y^2}\left(\hat{I}(x, y) - \widehat{\mu_L}\right) \tag{1}$$

Afterward, if the noise difference over the image is zero, it can be modified as follows.

$$\sigma_y^2 = 0 => \hat{\hat{I}} = \hat{I}(x, y) \tag{2}$$

In case, if the global noise difference is minimum and local difference is maximum [14], next the global difference develops to 1, and therefore,

If

$$\hat{\sigma}_y^2 \gg \sigma_y^2, then \hat{\hat{I}} = \hat{I}(x, y) \tag{3}$$

The superior local difference illustrates the happening of an edge to an image window. To same local and global difference, the notion is showed as:

$$\hat{I} = \widehat{\mu_L} as \hat{\sigma}_y^2 \approx \sigma_y^2 \tag{4}$$

The existing similarities depict a mean that the output represents the mean value of window with no disorders. It can be inherent functionality of WF. These filters utilize window size as the input and calculate residual objectives. Therefore, the gained outcomes suppose that the noise is removed from CXR image use of WF. An essential goal of this method is to identify the outcome of WF noise removal on edge.

3.2. Caps Net based Feature Extractor

Next to data pre-processing, Caps Net is employed for feature extraction purposes. The Caps Net is a new kind of NN presented as Hinton that utilizes the module length of activation vectors of the capsules for describing the probabilities of the presence of features and utilizes the way of activation vectors of the capsule for representing the parameter of the equivalent sample [15]. Different previous NNs that are comprised of neurons, capsule NNs with particular meaning and direction. The activation of neuronal activity in the capsule signifies different characteristics of particular features proposed in the image. At the network levels, the Caps Net has comprised of several layers. The minimum level capsule is known as vector capsule, and they can be utilized only a tiny part of an image as input correspondingly. The tiny area is named as perceptual domains. At superior levels, capsule is named routing capsules are utilized for detecting huge and more difficult objects. The outcomes of the capsules are vectors and the vector length signifies the evaluated probabilities of the presence of an object, and their way record the object of attitude parameter. When the object alters somewhat, the capsule is output vectors with a similar length but somewhat distinct way. Thus, the capsules are isotropic. Fig. 1 illustrates the structure of Capsule neural network.
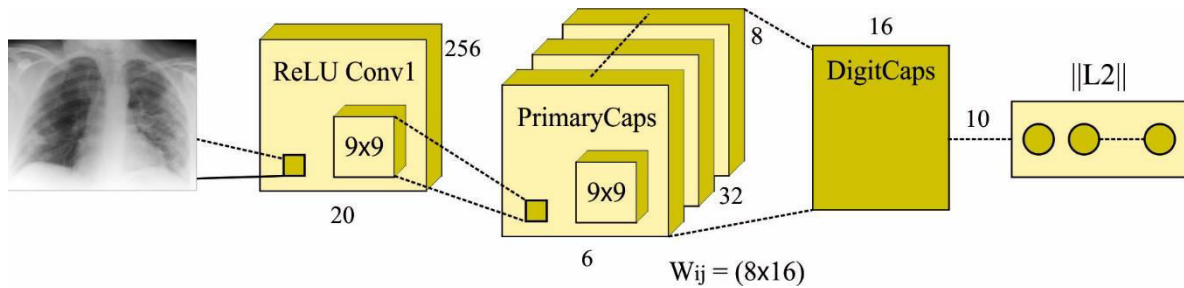
Fig. 1. Structure of Capsule Neural Network

3.3. Image Classification

The extracted feature vectors are fed into the DNN model to perform the classification process. The DNN model includes three major elements namely input, hidden, and output layers. With the consideration of the weight fitness values, the DNN is modeled by the use of 2 hidden layers to effectively learn the mapping function amongst the input as well as output data. Fig. 2 demonstrates the structure of DNN model. During the training process, the DNN model continually updates the node's weight in the hidden layer. With an increase in the number of rounds and to improve the training rate of the DNN model, 2 hidden layers are designed. At the hidden layer, the node count can be derived using Eq. (5):

$$n = \sqrt{a+b} + c \tag{5}$$

where $a\ and\ b$ indicates the input and output layer node count respectively, the number of hidden layer node was defined by n and a constant value amongst 1 to 10 is composed as c. To enable the non-linear fitness capability, sigmoid activation function is included using Eq. (6):

$$S = \frac{1}{1 + e^{-x}} \tag{6}$$

The input to the DNN model can be defined by x and it can be triggered using the mapping function M_f.

$$M_f = sigm(\omega_i x + \beta_i) \tag{7}$$

where ω and β signify the weight matrices and the biases among the output and hidden layers correspondingly [16]. Provided a abstractly labeled data instances (x, l) for a hidden layer, the loss procedure is defined by

$$S(W_s, b_s; x, l) = \frac{1}{2m} \sum_{j=1}^{m} \left\| h_j(W_s, b_s; x) - l_j \right\|_2^2 \tag{8}$$

where W_s and b_s denotes the bias and m indicate the neuron count in the hidden layers. Cross-entropy is employed for the loss function of DNN which considerably enhances the performance. It can be represented as follows.

$$C_E = \frac{1}{n} \sum_{k=1}^{n} \left[Y_k log \hat{Y}_k + (1 - Y_k) log(1 - \hat{Y}_k) \right] \tag{9}$$

where n characterizes training sample count, Y_k specifies the kth real outcome of the training set, $\hat{Y}_k$ is the kth predictable outcome of testing data.
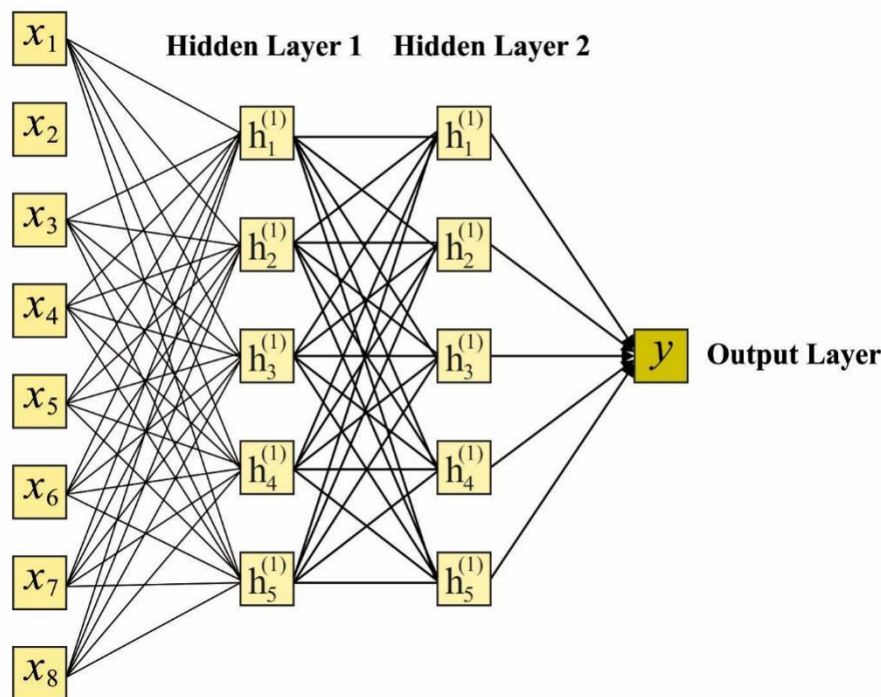
Fig. 2. Structure of DNN

In order to tune the hyperparameter involved in the DNN model, the IGWO algorithm is utilized. The GWO method is modelled according to hunting scenarios of gray wolves as presented in Mirjalili et al. [17]. Like another metaheuristic method, it can be population-based and iterative method. The social hierarchy and hunting approach of the wolf is employed for the numerical module. The modelling of GWO method has hunting, social hierarchy, attacking, and encircling preys.

Social hierarchy: In GWO method, it has alpha (α), beta (β), delta (δ), omega (ω) and all the wolves could have individual part of them. Based on GWO method, the optimal 3 locations of the population are allocated as delta beta, and alpha wolfs correspondingly. The remaining population is adopted that exists ω. The hierarchal dominance amongst the gray wolfs in swarm. The leader (alpha) mainly dominate the remaining population and make decision regarding social life; as rest place, hunting, time to wake, etc.

Encircling prey: The gray wolf surrounding its prey in the hunt. At the GWO algorithm, the wolf surrounding performance of prey is mathematically defined using Eq. (10).

$$X' = \vec{X} - A.D \qquad (10)$$

$$D = \left| \vec{C}.\vec{X} - X \right| \qquad (11)$$

Now $A \& \vec{C}$ denotes coefficient *vectors* $\rightarrow$ that is estimated using Eq. (12) $\rightarrow$ and Eq. (13) correspondingly. X_p represents location of the prey, and X indicates present location of the gray wolf.

$$\vec{A} = 2.\alpha.\vec{r}_1 - \alpha \qquad (12)$$

$$\vec{C} = 2.\vec{r} \qquad (13)$$

whereas α denotes real number (it can be value of continuous quantity which could denote a distance beside a line) that is consecutively decreased from two to zero based on the amount of iteration, and $\vec{r}_1, \vec{r}_2$ denotes real number array arbitrarily made in [0,1]. For seeing the consequence of Eq. (10), the probable subsequent position of gray wolves [18].

Hunting: As stated earlier, the leader wolves ($\alpha, \beta \& \delta$) have an optimal position in population and the hunting is mainly directed with them. Omega wolfs upgrade the location to the probable prey that is defined using $\alpha, \beta \& \delta$. In GWO, hunting performance of the wolf is numerically modelled by Eqs. (14)-(16).

$$\overrightarrow{D_\alpha} = \left| \vec{C}_1.\vec{X}_\alpha - \vec{X} \right|$$

$$\overrightarrow{D_\beta} = \left| \vec{C}_2.\vec{X}_\beta - \vec{X} \right| \qquad (14)$$

$$D_\delta = \left| \vec{C}_3.\vec{X}_\delta - \vec{X} \right|$$

$$\overrightarrow{X_1} = \vec{X}_\alpha - \overrightarrow{A_1}.\overrightarrow{D_\alpha}$$

$$\overrightarrow{X_2} = \vec{X}_\beta - A_2.\overrightarrow{D_\beta} \qquad (15)$$

$$\overrightarrow{X_3} = \vec{X}_\delta - A_3.\overrightarrow{D_\delta}$$

$$X' = \frac{\vec{X}_1 + \vec{X}_2 + \vec{X}_3}{3} \qquad (16)$$

Attacking: In last phase, the wolf select among attack the prey and search the optimal novel prey. It is called that α is a real number that consecutively reduces from two to zero based on iteration amount. Eq. (12) displays the value of vector A$\rightarrow$ is reduced based on α. Therefore, based on reducing of α, A is a vector of arbitrarily created real numbers among $-2\alpha \& 2\alpha$. The wolf attacks the prey if $|A| < 1$ when $|A| > 1$ feasibly choose for searching a fitter prey.

A significant characteristic of DE is the mutation operation. If the individual is chosen, 2 variations with the weights are included to the individual to attain the variation. The fundamental element of DE is the difference vector of the parent, and every individual vector encompasses a pair of distinct individuals (X_{r1}^t, X_{r2}^t) of parents. The difference vector can be represented as follows.

$$\mathrm{D}d_{r12} = X_{r1}^t - X_{r2}^t \qquad (17)$$

where, r_1, r_2 expresses indices of distinct individuals in the populations [19]. Therefore, the mutation function is defined by:

$$V_i^{t+1} = X_{r3}^t + F * (X_{r1}^t - X_{r2}^t) \qquad (18)$$

where, $r_1 - r_3$ are dissimilar integers. For producing an ideal difference factors for verifying that the wolf evolves in the course that is better for their developments. So, this work selects the outperforming individuals of wolves as parents. Once several simulation processes are performed, the β and δ ones are chosen as 2 parents, and then integrated into the α wolf to procedure a variance factors, as defined below

$$V_j^{t+1} = X_\alpha^t + F * \left(X_\beta^t - X_\delta^t \right) \tag{19}$$

To accomplish maximum exploration capability in the earlier level to avoid local optima problems, a dynamic scaling factor F is applied, which changes from high to low value based on the iteration number in Eq. (20).

$$F = f_{\min} + (f_{\max} - f_{\min}) \times \frac{\text{Max}\_iter - (iter - 1)}{\text{Max}\_iter} \tag{20}$$

where, $f_{\min}$ and $f_{\max}$ are the lower and higher values of the scaling factor.

4. Performance Validation

The experimental validation of the AIHA-DNN method takes place using the benchmark CXR dataset [20]. The dataset includes images from different classes namely Normal, COVID-19, SARS, and Pneumocystis. Fig. 3 illustrates the sample test images.
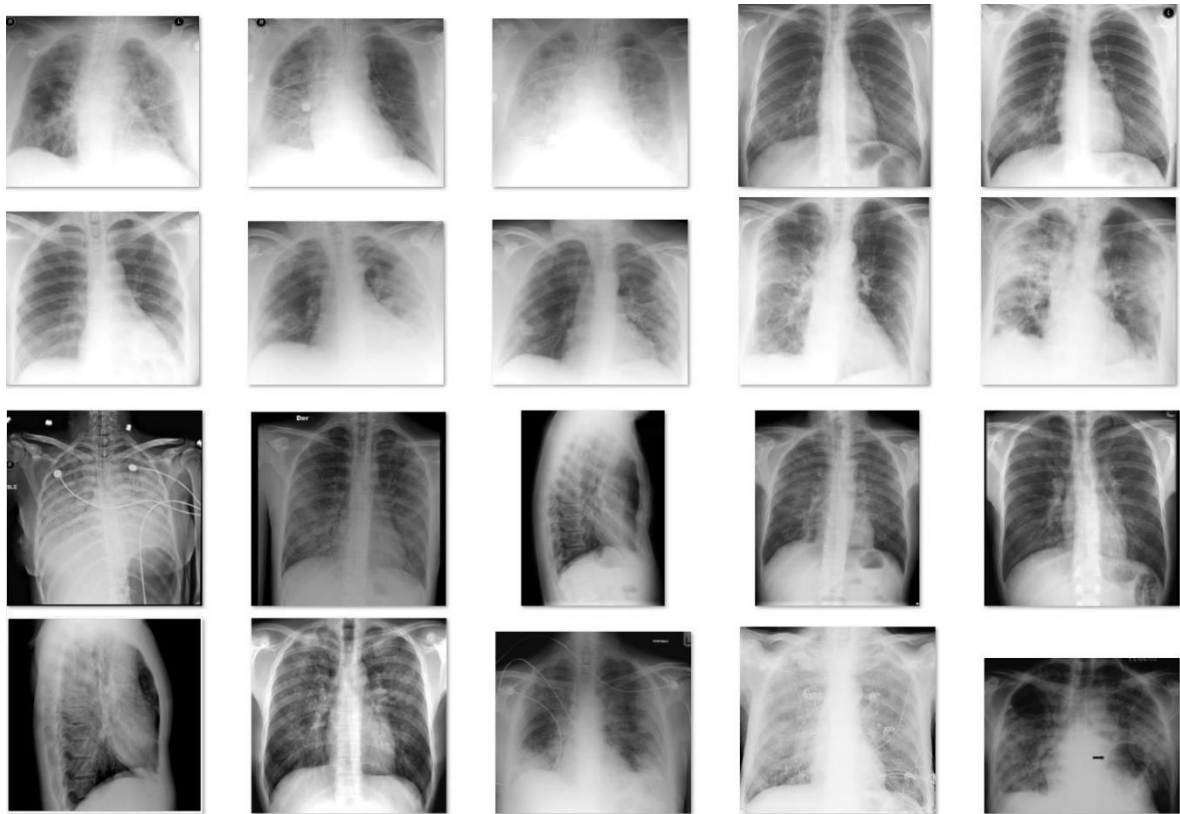
Fig. 3. Sample Images

The classification performance of the AIHA-DNN model takes place under varying number of folds in Table 1. The results showcased that the AIHA-DNN model has accomplished enhanced outcomes over all the folds. For instance, with fold-1, the AIHA-DNN technique has obtained an increased classification performance with the sensitivity of 98.54%, specificity of 96.58%, accuracy of 98.91%, F1-score of 96.50%, and kappa of 96.46%. Eventually, with fold-3, the AIHA-DNN approach has attained a higher classification with the sensitivity of 96.92%, specificity of 95.80%, accuracy of 95.95%, F1-score of 99.09%, and kappa of 97.51%. Meanwhile, with fold-5, the AIHA-DNN manner has gained an improved classification efficinecy with the sensitivity of 96.84%, specificity of 95.83%, accuracy of 95.67%, F1-score of 95.95%, and kappa of 95.93%. Simultaneously, with fold-7, the AIHA-DNN method has reached a maximal classification outcom with the sensitivity of 99.13%, specificity of 95.63%, accuracy of 95.57%, F1-score of 97.80%, and kappa of 97.43%. Concurrently, with fold-10, the AIHA-DNN methodology has achieved a superior classification efficiency with

the sensitivity of 98.05%, specificity of 97.83%, accuracy of 97.55%, F1-score of 97.99%, and kappa of 97.08%.

Table 1 Result Analysis of AIHA-DNN Method with respect to distinct Measures

No. of Folds	Sensitiv ity	Specific ity	Accura cy	F1-Score	Kappa
Fold-1	98.54	96.58	98.91	96.50	96.46
Fold-2	98.07	97.44	98.91	97.90	98.09
Fold-3	96.92	95.80	95.95	99.09	97.51
Fold-4	98.44	96.88	99.13	95.61	96.68
Fold-5	96.84	95.83	95.67	95.95	95.93
Fold-6	97.18	96.94	97.54	95.86	98.13
Fold-7	99.13	95.63	95.57	97.80	97.43
Fold-8	97.03	96.54	98.78	97.82	97.60
Fold-9	96.69	97.03	98.06	95.86	95.91
Fold-10	98.05	97.83	97.55	97.99	97.08
Average	**97.69**	**96.65**	**97.61**	**97.04**	**97.08**
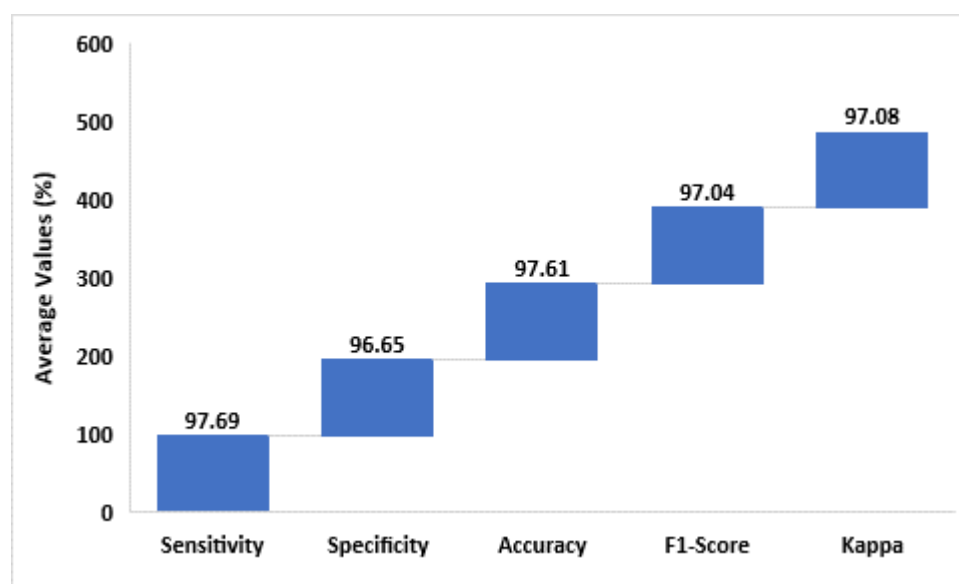
Fig. 4. Average analysis of AIHA-DNN model with different measures

Fig. 4 depicts the average classification results analysis of the AIHA-DNN technique. The figure demonstrated that the AIHA-DNN technique has resulted to a maximum average sensitivity of 97.69%, specificity of 96.65%, accuracy of 97.61%, F-score of 97.04%, and kappa of 97.08%.
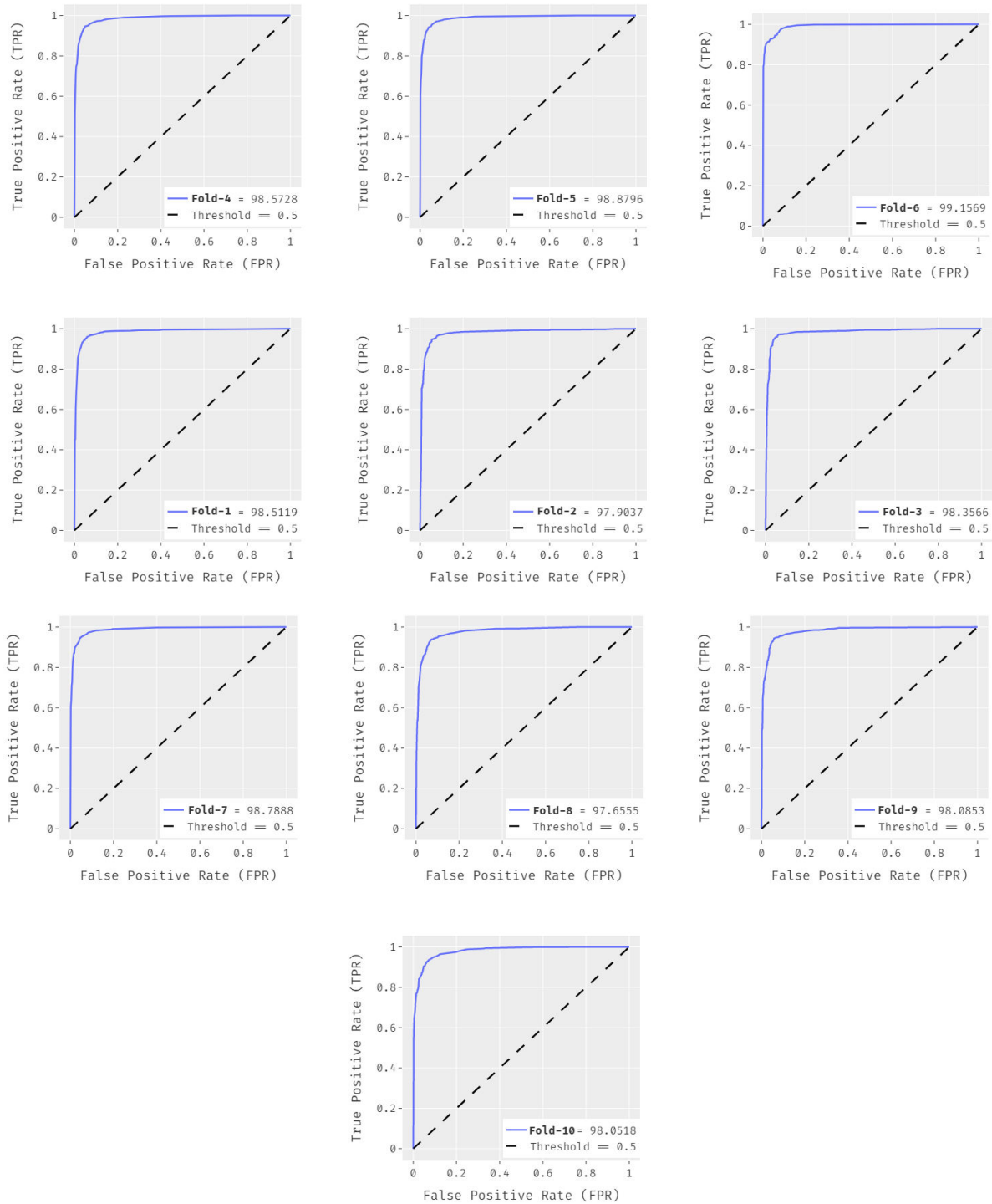
Fig. 5. ROC Analysis of AIHA-DNN model on 10-Folds

Fig. 5 illustrates the ROC analysis of the AIHA-DNN technique under distinct folds. From the figure, it is evident that the AIHA-DNN technique has accomplished effectual outcomes with the maximum ROC value under all the folds.

In order to ensure the improved performance of the AIHA-DNN technique over the other techniques, a brief comparison study is made in Table 2 and Fig. 6 [21].

Table 2 Comparison study of AIHA-DNN technique on CXR dataset

Methods	Sensitivity	Specificity	Accuracy	F-score
AIHA-DNN	0.9769	0.9665	0.9761	0.9704
FM-HCF-DLF	0.9361	0.9456	0.9408	0.932
Conv. NN	0.8773	0.8697	0.8736	-
DT Learning	0.8961	0.9203	0.9075	-
ANN Classifier	0.8745	0.8291	0.8509	-
ANFIS	0.8848	0.8774	0.8811	-
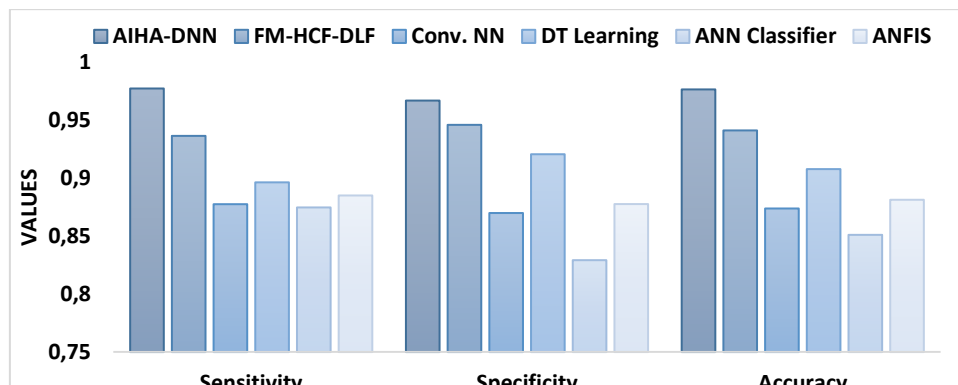
Fig. 6. Comparative analysis of AIHA-DNN model with existing techniques

From the results, it is apparent that the ANN classifier model has showcased insufficient performance with the least accuracy of 0.8509 whereas the Conv. NN model has gained slightly improved outcomes with an accuracy of 0.8736. Followed by, the ANFIS model has demonstrated moderate performance with an accuracy of 0.8811. Concurrently, the DT learning and FM-HCF-DLF techniques have obtained reasonable outcomes with closer accuracy of 0.9075 and 0.9408 respectively. However, the AIHA-DNN method has resulted in maximal classification performance with a supreme accuracy of 0.9761. The aforementioned tables and figures verified the effectual diagnostic performance of the AIHA-DNN technique on COVID-19 diagnosis and classification.

5. Conclusion

This paper has presented a novel AIHA-DNN technique to detect and classify COVID-19 utilizing CXR image. The presented AIHA-DNN method encompasses WF based pre-processing, Squeeze Net based feature extraction, DNN based classification, and IGWO based parameter adjustment. The IGWO algorithm is derived by the inclusion of mutation operator into the conventional GWO algorithm and the hyper parameter adjustment of the DNN model assists to accomplish maximum detection rate. The experimental analysis of the AIHA-DNN technique is performed on benchmark CXR datasets and the outcomes are assessed with respect to distinct evaluation parameters. The experimental results highlighted the enhanced diagnostic performance of the AIHA-DNN technique over the recent methods with the maximum sensitivity, specificity, and accuracy of 97.69%, 96.65%, and 97.61% respectively. In future, the COVID-19 diagnostic performance can be improved by the use of hybrid DL models.

References

Brunese, L., Mercaldo, F., Reginelli, A. and Santone, A., 2020. Explainable deep learning for pulmonary disease and coronavirus COVID-19 detection from X-rays. Computer Methods and Programs in Biomedicine, 196, p.105608.

C. Huang, Y. Wang, et al., Clinical features of patients infected with 2019 novel coronavirus in Wuhan, China, Lancet 395 (10223) (2020) 497–506.

C. Long, H. Xu, et al., Diagnosis of the Coronavirus disease (COVID-19): rRT-PCR or CT? Eur. J. Radiol. 126 (2020) 108961.

F. Wu, S. Zhao, B. Yu, et al., A new coronavirus associated with human respiratory disease in China, Nature 579 (7798) (2020) 265–269.

F. Pan, T. Ye, et al., Time course of lung changes on chest CT during recovery from 2019 novel coronavirus (COVID-19) pneumonia, Radiology (2020).

https://github.com/ieee8023/covid-chestxray-dataset

Jain, R., Gupta, M., Taneja, S. and Hemanth, D.J., 2021. Deep learning based detection and analysis of COVID-19 on CXR images. Applied Intelligence, 51(3), pp.1690-1700.

Karakoyun, M., Ozkis, A. and Kodaz, H., 2020. A new algorithm based on gray wolf optimizer and shuffled frog leaping algorithm to solve the multi-objective optimization problems. *Applied Soft Computing*, *96*, p.106560.

Loey, M., Manogaran, G., Taha, M.H.N. and Khalifa, N.E.M., 2021. A hybrid deep transfer learning model with machine learning methods for face mask detection in the era of the COVID-19 pandemic. Measurement, 167, p.108288.

Ozturk, T., Talo, M., Yildirim, E.A., Baloglu, U.B., Yildirim, O. and Acharya, U.R., 2020. Automated detection of COVID-19 cases using deep neural networks with X-ray images. Computers in biology and medicine, 121, p.103792.

Pathak, Y., Shukla, P.K., Tiwari, A., Stalin, S. and Singh, S., 2020. Deep transfer learning based classification model for COVID-19 disease. Irbm.

Pustokhin, D.A., Pustokhina, I.V., Dinh, P.N., Phan, S.V., Nguyen, G.N. and Joshi, G.P., 2020. An effective deep residual network based class attention layer with bidirectional LSTM for diagnosis and classification of COVID-19. *Journal of Applied Statistics*, pp.1-18.

Ramesh, S. and Vydeki, D., 2020. Recognition and classification of paddy leaf diseases using Optimized Deep Neural network with Jaya algorithm. *Information processing in agriculture*, *7*(2), pp.249-260.

S. Mirjalili, S.M. Mirjalili, A. Lewis, Grey.wolf. optimizer, Grey wolf optimizer, Adv. Eng. Softw. 69 (2014) 46–61.

Shah, V., Keniya, R., Shridharani, A., Punjabi, M., Shah, J. and Mehendale, N., 2021. Diagnosis of COVID-19 using CT scan images and deep learning techniques. Emergency radiology, 28(3), pp.497-505.

Shankar, K. and Perumal, E., 2020. A novel hand-crafted with deep learning features based fusion model for COVID-19 diagnosis and classification using CXR images. *Complex & Intelligent Systems*, pp.1-17.

Shankar, K., Perumal, E., Tiwari, P., Shorfuzzaman, M. and Gupta, D., 2021. Deep learning and evolutionary intelligence with fusion-based feature extraction for detection of COVID-19 from CXR images. *Multimedia Systems*, pp.1-13.

T. Singhal, A review of coronavirus disease-2019 (COVID-19), Indian J. Pediatr. 87 (2020) 281–286.

Wang, Z., Zheng, L., Du, W., Cai, W., Zhou, J., Wang, J., Han, X. and He, G., 2019. A novel method for intelligent fault diagnosis of bearing based on capsule neural network. *Complexity*, *2019*.

Wang, J.S. and Li, S.X., 2019. An improved grey wolf optimizer based on differential evolution and elimination mechanism. *Scientific reports*, *9*(1), pp.1-21.

Z.Y. Zu, M.D. Jiang, P.P. Xu, W. Chen, Q.Q. Ni, G.M. Lu, L.J. Zhang, Coronavirus disease 2019 (COVID-19): a perspective from China, Radiology (2020